



Title	Effect of particle size on the oxygen reduction reaction activity of carbon - supported niobium-oxide - based nanoparticle catalysts
Author(s)	Shinyoshi, Naoki; Seino, Satoshi; Hasegawa, Yuta et al.
Citation	Journal of Materials Science. 2025, 60, p. 3275-3285
Version Type	VoR
URL	https://hdl.handle.net/11094/100450
rights	This article is licensed under a Creative Commons Attribution 4.0 International License.
Note	


The University of Osaka Institutional Knowledge Archive : OUKA

<https://ir.library.osaka-u.ac.jp/>

The University of Osaka



Effect of particle size on the oxygen reduction reaction activity of carbon-supported niobium-oxide-based nanoparticle catalysts

Naoki Shinyoshi¹, Satoshi Seino^{1,*} , Yuta Hasegawa¹, Yuta Uetake^{2,3}, Takaaki Nagai⁴, Ryuji Monden⁴, Akimitsu Ishihara⁴, and Takashi Nakagawa¹

¹ Management of Industry and Technology, Graduate School of Engineering, Osaka University, 2-1 Yamadaoka, Suita, Osaka 565-0871, Japan

² Division of Applied Chemistry, Graduate School of Engineering, Osaka University, 2-1 Yamadaoka, Suita, Osaka 565-0871, Japan

³ Innovative Catalysis Science Division, Institute for Open and Transdisciplinary Research Initiatives, Osaka University, 2-1 Yamadaoka, Suita, Osaka 565-0871, Japan

⁴ Institute of Advanced Sciences, Yokohama National University, 79-5 Tokiwadai Hodogaya-ku, Yokohama 240-8501, Japan

Received: 7 November 2024

Accepted: 7 January 2025

Published online:
3 February 2025

© The Author(s), 2025

ABSTRACT

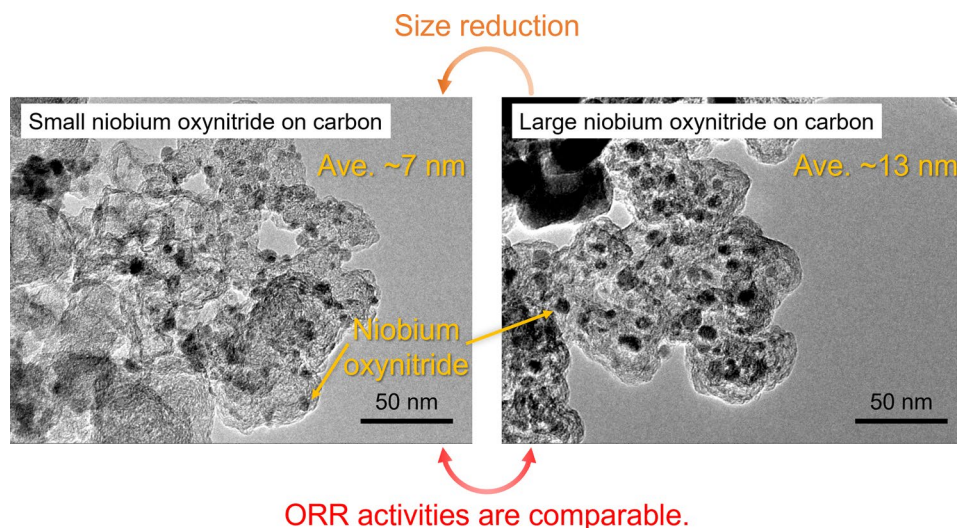
In this study, niobium oxynitride nanoparticles were examined to determine the effect of particle size on oxygen reduction reaction (ORR) activity. To this end, catalyst precursors with niobium oxides dispersed on carbon supports were prepared using the irradiation or impregnation method. Polyacrylonitrile was added to each precursor, followed by heat treatment under an ammonia-containing atmosphere to synthesize niobium oxynitride nanoparticles. The structures of the prepared catalysts were analyzed using transmission electron microscopy, X-ray diffraction, and X-ray absorption spectroscopy. The results indicated that two catalysts with the same crystal phase but different particle sizes were obtained. Comparing their ORR activities revealed that the effect of particle size on ORR activity was limited. Thus, it was inferred that controlling the microelectron conduction paths can help maximize the benefits of particle size reduction. In addition, niobium oxynitride nanoparticles with different structures were obtained by varying the heat-treatment temperatures, and the ORR activity of each prepared catalyst was evaluated. These findings suggest that forming graphitized carbon residues with high electrical conductivity and controlling nitrogen-doping in the oxide nanoparticles are crucial steps for enhancing the ORR activity of oxide-based catalysts. These findings offer valuable insights for developing material design strategies to improve oxide-based catalyst performance.

Handling Editor: Pedro Camargo.

Address correspondence to E-mail: seino@mit.eng.osaka-u.ac.jp

<https://doi.org/10.1007/s10853-025-10632-z>

GRAPHICAL ABSTRACT



Introduction

Polymer electrolyte fuel cells (PEFCs) are considered promising energy-conversion devices because of their high energy efficiency and low environmental impact; however, the widespread adoption of PEFCs is limited by the high cost of platinum catalysts used for the oxygen reduction reaction (ORR) at the cathode [1, 2]. Platinum-free catalysts have been extensively researched to overcome this limitation [3–5]. To this end, metal oxide catalysts based on group IV and group V elements have been widely explored [6–8] because they offer advantages such as high chemical stability under acidic conditions, cost-effectiveness, and abundant availability. The ORR activity of these catalysts is lower than that of platinum-based catalysts, and therefore, identifying structural factors contributing to their high activity and establishing optimal design guidelines is necessary.

One of the key limitations of oxide-based catalysts is their low electrical conductivity, which hinders electron transfer during electrode reactions, reducing current density [7, 9]. Effectively forming electron conduction paths within the catalyst to facilitate efficient electron transfer from the electrode to the active sites on the oxide surface is necessary to mitigate this issue. Macroelectron conduction paths, defined as those between the electrode and oxide particles, and microelectron conduction paths, defined as those between the support and active sites, need to be optimized [10].

The macroelectron conduction paths depend on the conductive support that carries the oxide particles, while the microelectron conduction paths are determined by carbon residues formed at the interface between the oxide particles and support (Fig. 1). Oxide-based catalysts are synthesized by preparing suitable catalyst precursors followed by heat treatment under specific conditions. In our previous study, polyacrylonitrile (PAN) was heat-treated together with the catalyst precursor, which led to the formation of carbon residues that served as microelectron conduction paths, thereby increasing the current density [11]. Other structural factors such as the crystal phase and particle size of the oxides can also affect the ORR activity. However, the independent control of these factors remains challenging, and their respective contributions to the ORR activity are yet to be fully

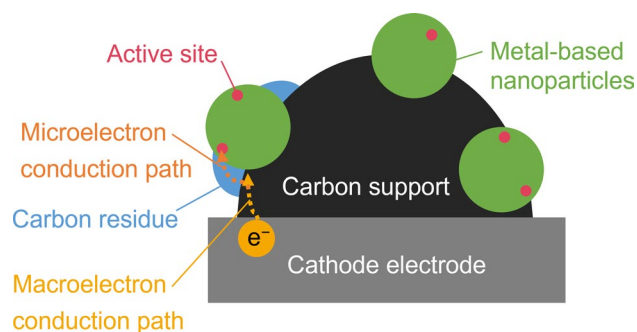


Figure 1 Schematic of the catalyst structure and electron conduction paths.

understood. Therefore, the clarification of these factors is crucial to create design guidelines for oxide-based catalysts with high ORR activity, ultimately improving the performance of platinum-free catalysts.

Reducing the particle size of oxides increases the specific surface area, which can potentially enhance the number of active sites and improve catalytic performance. However, conventional synthetic methods for oxide-based catalysts are difficult to control particle size, due to the heat-treatment process, during which particle growth is observed. Further, the ORR activity is affected not only by the specific surface area but also by factors such as electron conduction paths and the crystal phase of oxide particles, which makes it difficult to definitively assess the effect of particle size on the ORR activity. To address this issue, an irradiation method was proposed by our research group. The irradiation method is a nanoparticle synthesis technique that utilizes chemical reactions induced by radiation to control particle size. This method can ensure the uniform dispersion of ~ 3 nm niobium oxide particles on carbon supports [11]. Furthermore, catalysts obtained by heat-treating this sample as a precursor exhibit high dispersion, which suppresses particle growth during heat treatment. Therefore, niobium oxides with different particle sizes can be deposited on the carbon surface by selectively using either the conventional or irradiation method to prepare the catalyst precursors.

In this study, we focused on niobium oxynitride nanoparticles and investigated the effect of particle size on the ORR activity. Catalyst precursors with niobium oxide nanoparticles dispersed on carbon supports were prepared using the irradiation or impregnation method. The catalyst precursors were then heat-treated to synthesize niobium oxynitride nanoparticles with different particle sizes. Previous studies reported that heat treatment under an ammonia atmosphere can lead to slight nitrogen-doping of niobium oxides on carbon, improving the ORR activity [12]. Therefore, this study aimed to enhance the catalytic activity by introducing nitrogen-doping into niobium oxides through heat treatment in an ammonia-containing atmosphere [12–14]. In addition, relationships between the degree of nitrogen-doping, the state of the microelectron conduction paths, and their effect on the ORR activity were evaluated. This study enhances the understanding of the factors influencing ORR activity in oxide-based catalysts and provides design guidelines for improving their performance.

Experimental

Catalyst synthesis

Ultrapure water (≥ 18 M Ω cm, Millipore Direct-Q UV) was used as the solvent, and 2-propanol ($\geq 99.5\%$, FUJIFILM Wako Pure Chemical Corp., Japan) was used as a scavenger for hydroxyl radicals. An aqueous solution of niobium(V) oxalate (100%, H. C. Starck GmbH) was used as the metal oxide precursor. Carbon black powder (Nippon Ketjen Co., Ltd., BET surface area: $800\text{ m}^2\text{ g}^{-1}$) was used as the support.

The catalyst precursors were prepared using the irradiation or impregnation method. The catalyst precursors were prepared via the irradiation method as follows: Aqueous solutions of niobium ions were prepared at a concentration of 2 mmol dm^{-3} and then mixed with 2-propanol (1 vol.%) and carbon support. The loading amount of niobium was controlled to two-thirds of the weight of the carbon support, calculated as the metallic niobium equivalent, by adjusting the amount of carbon support. The precursor solution (200 cm^3 per sample) was transferred to a glass vial (No. 10, Maruemu Corp.), mixed thoroughly, and sonicated for 30 min. Argon gas was bubbled through the mixture to remove the dissolved oxygen from the solution. Each vial containing the mixture was irradiated with ^{60}Co gamma radiation at a total absorbed dose of $\sim 100\text{ kGy}$ at a commercial facility (Koga Isotope, Ltd.). Subsequently, the irradiated samples were suction-filtered, washed with ultrapure water, and dried in air at 60°C overnight to obtain the catalyst precursors (“as irradiated”) in powder form (ca. 18 wt.% calculated as the metallic niobium equivalent). This value is expected to remain largely unchanged even after heat treatment. These catalyst precursors were mixed with PAN (M.W. = 150,000, Sigma-Aldrich Japan Co. LLC) in *N,N*-dimethylformamide (70 cm^3 , DMF; $\geq 99.5\%$, FUJIFILM Wako Pure Chemical Corp., Japan) at a mass ratio of 1:1 and sonicated for 45 min. The mixtures were then dried under vacuum at 60°C to obtain the powder samples. These samples were subsequently heat-treated to 800, 900, and 1000°C (at a set heating rate of $800\text{--}1000^\circ\text{C min}^{-1}$) for 3 h in an atmosphere containing 50% NH_3 and 0.3% O_2 with N_2 as the balance gas at the flow rate of $350\text{ cm}^3\text{ min}^{-1}$, for 3 h.

Another catalyst precursor was prepared using the impregnation method, followed by oxidation, and then the catalyst was synthesized from the precursor using the same procedure as that for the irradiation

method. Niobium(V) oxalate and carbon black powder were mixed thoroughly in ethanol (50 cm^3 , $\geq 99.5\%$, FUJIFILM Wako Pure Chemical Corp., Japan) in a glass vial (No. 8, AS ONE Corp.), and sonicated for 30 min. The loading amount of niobium was controlled in a manner similar to that for the irradiated samples. The impregnated sample was dried under vacuum at $60\text{ }^\circ\text{C}$ to obtain a powder sample. As pretreatment, the powder sample was oxidized at $700\text{ }^\circ\text{C}$ (heating rate of $700\text{ }^\circ\text{C min}^{-1}$) for 1 h in an atmosphere containing 0.1% O_2 with N_2 as the balance gas. The oxidized powder served as the catalyst precursor (“impregnated”, ca. $23\text{ wt.}\%$ calculated as the metallic niobium equivalent). This catalyst precursor was mixed with PAN in DMF (70 cm^3) at a mass ratio of 1:1, sonicated, and dried under vacuum at $60\text{ }^\circ\text{C}$ to obtain a powder sample. This sample was then heat-treated at $800\text{ }^\circ\text{C}$ (heating rate of 800 min^{-1}) for 3 h in an atmosphere containing 50% NH_3 and 0.3% O_2 with N_2 as the balance gas.

Characterization

The morphologies of the catalysts were examined using transmission electron microscopy (TEM; JEM-2100, JEOL Ltd., 200 kV). For the TEM measurements, the samples were suspended in ultrapure water by ultrasonication for 1 min, and a few drops of the suspension were cast onto carbon-coated copper grids (Cat. 653, Nisshin-EM Corp.), followed by overnight drying in air at $60\text{ }^\circ\text{C}$. The crystalline structure was analyzed using X-ray diffraction (XRD; MiniFlex 600, Rigaku Corp., 40 kV , 15 mA) with $\text{Cu-K}\alpha$ radiation in the continuous scan mode. The XRD patterns were compared with the JCPDS databases (File no. 30-873, 42-1125, 38-1155, and 38-1364) to identify the phases in the samples. Nb K-edge X-ray absorption spectroscopy (XAS) measurements were taken at the NW-10A beamline of KEK using the transmission method. The chemical composition ratios were estimated via the linear combination fitting analysis of the XAS spectra, using Nb foil, NbO , Nb_2O_3 , NbO_2 , Nb_2O_5 , NbN , and NbC as references. The weight of Nb in the catalysts was determined by X-ray fluorescence (XRF; Shimadzu Corp., Rayny EDX-720) analysis. The samples for the measurements were prepared by mixing the catalyst with ZnO (Adachi New Industrial Co.) as an internal standard at a mass ratio of 1:1.

Electrochemical measurement

Electrochemical measurements were taken as discussed in another paper [10]. The measurements were taken using a stationary electrode system instead of a rotating electrode system [11, 15, 16]. Catalyst powder (2.0 mg) was mixed with 1-hexanol (200 mm^3) and Nafion[®] solution ($1.0\text{ wt.}\%$, 10 mm^3) to prepare catalyst ink. The Nafion[®] solution was prepared by diluting a Nafion[™] dispersion solution ($5.0\text{--}5.4\text{ wt.}\%$, DE520 CS type, FUJIFILM Wako Pure Chemical Corp., Japan) with ultrapure water and 1-propanol at a 1:1 mass ratio. The catalyst ink was dropped on a polished glassy carbon rod (GC; $\varphi = 5.2\text{ mm}$, Tokai Carbon Co., Ltd.) and dried at $60\text{ }^\circ\text{C}$ for 30 min. The catalyst loading was set as $\sim 0.5\text{ mg}_{\text{catalyst}}\text{ cm}^{-2}$ on top of the GC.

A static three-electrode cell in $0.5\text{ mol dm}^{-3}\text{ H}_2\text{SO}_4$ (for volumetric analysis, factor = 1000, FUJIFILM Wako Pure Chemical Corp., Japan), and a potentiostat was used for the measurements. A reversible hydrogen electrode (RHE) and GC plate were used as the reference and counter electrodes, respectively. The cell temperature was maintained at $30\text{ }^\circ\text{C}$ during the measurements. Before the measurements, the electrode underwent 200 cycles of potential sweeping between 0.05 and 1.1 V under an O_2 atmosphere to ensure cleanliness. Slow scan voltammetry (SSV) was conducted at a scan rate of 5 mV s^{-1} between 0.2 and 1.1 V under both O_2 and N_2 atmospheres. The purities of the O_2 and N_2 gases were higher than 99.5% and 99.99995% , respectively. The ORR current density (i_{ORR}) was calculated by subtracting the current density under the N_2 atmosphere from that under the O_2 atmosphere. The rest potential (E_{rest}) under the O_2 atmosphere was determined by holding the electrode undisturbed for 1 h. Cyclic voltammetry (CV) was performed at a scan rate of 50 mV s^{-1} in the range of $0.05\text{--}1.2\text{ V}$ under an N_2 atmosphere. In this study, i_{ORR} and E_{rest} were used as indicators of ORR activity.

Material characterization

Effect of precursor preparation method on catalyst structure

Catalyst precursors prepared using the irradiation or impregnation method were heat-treated, and the material characteristics of the resulting catalysts were compared. In both cases, heat treatment was

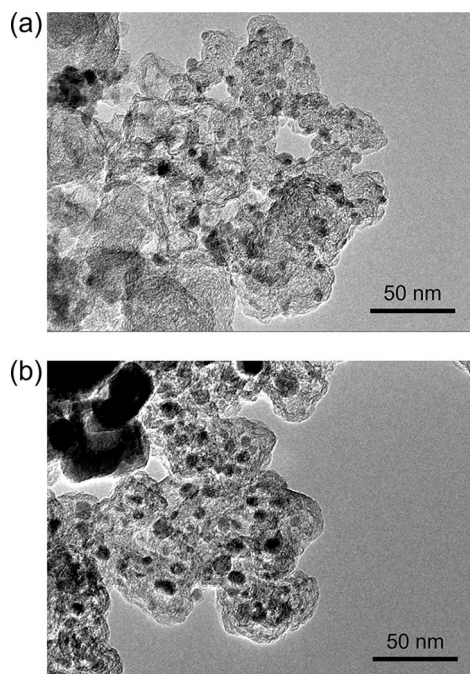


Figure 2 TEM images of the samples obtained from heat treatment of the precursors: **a** “as irradiated” and **b** “impregnated” precursor.

conducted at 800 °C for 3 h in an ammonia-containing gas atmosphere to synthesize the catalysts.

The TEM images of the samples obtained from the heat treatment of each precursor are shown in Fig. 2. In both samples, niobium-based nanoparticles were dispersed on the surface of the carbon supports. The average particle size of niobium-based nanoparticles was calculated from the observed fields: ~ 7 nm for the sample from the “as irradiated” precursor and 13 nm for that from the “impregnated” precursor, indicating a clear difference in particle size. The XRD patterns of the heat-treated samples are shown in Fig. 3. Both samples exhibited diffraction patterns corresponding to those of niobium oxynitride. The crystallite size calculated using Scherrer’s equation for diffraction peaks corresponding to the (111) planes of NbO and NbN (ca. $2\theta = 36^\circ$) was ~ 9 and 30 nm for the samples from the “as irradiated” and “impregnated” precursors, respectively. The discrepancy between the TEM results and crystallite sizes obtained from the XRD results can be attributed to the presence of coarser particles that were not visible within the observed TEM field of view. However, the relative particle sizes observed by TEM were consistent with the qualitative trends in XRD, suggesting

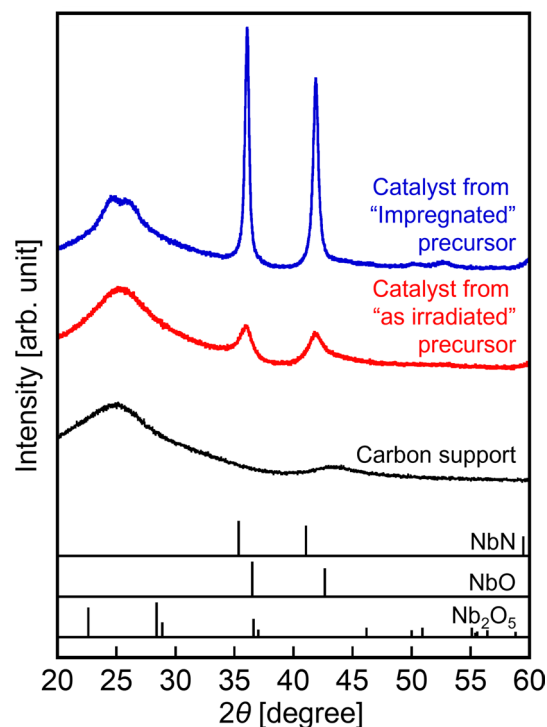


Figure 3 XRD patterns of the samples obtained from the heat treatment of each precursor.

that the results are sufficiently reliable for a qualitative discussion. In addition, assuming $\text{NbO}_x\text{N}_{1-x}$ based on Vegard’s law, the calculated x values were 0.42 and 0.43 for the samples from the “as irradiated” and “impregnated” precursors, respectively, indicating no significant difference in the crystal phase [17]. These results demonstrate that two catalysts with distinctly different niobium oxynitride particle sizes but the same crystal phase can be obtained by selectively using the irradiation or impregnation method for precursor preparation. This finding provides the basis for comparing the effect of particle size on ORR activity.

Effect of heat-treatment temperature on the catalyst structure

The material characteristics of the catalysts synthesized at different heat-treatment temperatures were compared. These catalysts were synthesized by heat-treating the “as irradiated” precursor at 800, 900, or 1000 °C for 3 h in an ammonia-containing gas atmosphere.

The TEM images of the samples heat-treated at different temperatures are presented in Fig. 4.

Although niobium-based nanoparticles were dispersed on the surface of the carbon support in all samples, a significant aggregation was observed at 1000 °C. In addition, the average particle size of niobium-based nanoparticles increased with increasing treatment temperature. The XRD patterns of the samples heat-treated at different temperatures are shown in Fig. 5. The diffraction patterns corresponding to niobium oxynitride were observed regardless of the treatment temperature. In addition, the intensity of the niobium oxynitride diffraction peaks increased with an increase in the treatment temperature, and the peak position shifted to lower angles in the sample treated at 1000 °C. Assuming $\text{NbO}_x\text{N}_{1-x}$ based on Vegard's law, the calculated x values were 0.42 and 0.39 at 800 and 900 °C, respectively, indicating a similar level of nitrogen-doping. In contrast, at 1000 °C, x decreased to 0.27, suggesting that the nitrogen-doping of the niobium oxide particles progressed further. Figure 6 shows the normalized Nb-K edge X-ray absorption near edge structure (XANES) spectra of the samples heat-treated at different temperatures. Compared to the sample treated at 800 °C, the peak intensity at ~18990 eV, which is characteristic with Nb_2O_5 , decreased for the samples heat-treated at 900 and 1000 °C, indicating a lower proportion of Nb_2O_5 . The chemical compositions of the catalysts, calculated from linear combination fitting analysis, are presented in Table 1. Unlike the sample treated at 800 °C, the ratio of Nb_2O_5 decreased and the ratios of NbO and NbN increased for samples treated at 900 and 1000 °C. These results indicate that higher heat-treatment temperatures promote the formation of low valent niobium species and increase the degree of nitrogen-doping on niobium oxide particles.

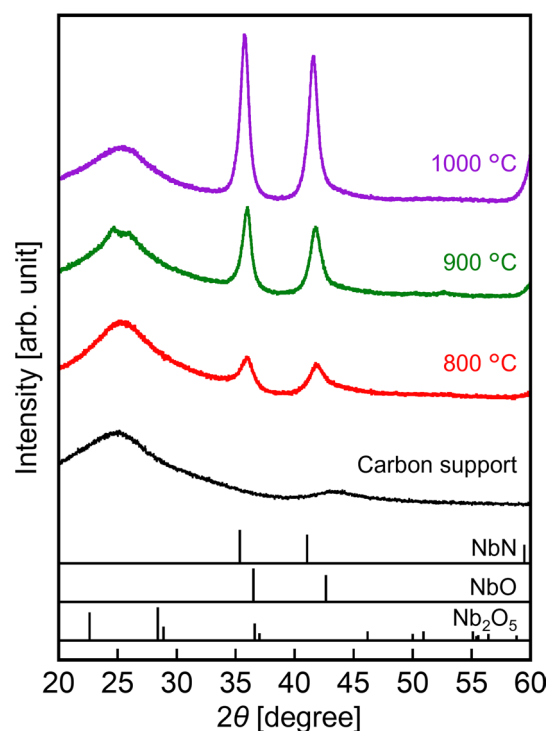


Figure 5 XRD patterns of the samples obtained by heat-treating the “as irradiated” precursor at different temperatures.

Discussions

Effect of particle size on the oxygen reduction reaction activity

The relationship between the size of niobium-based nanoparticles and the ORR activity is examined by comparing the samples analyzed in “Effect of precursor preparation method on catalyst structure” section. The correlation between the particle size and ORR

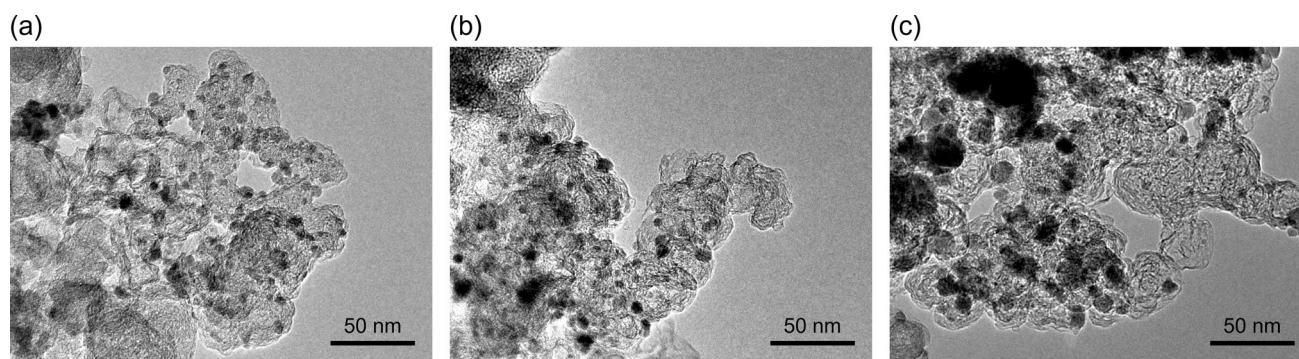


Figure 4 TEM images of the samples obtained by heat-treating the “as irradiated” precursor at **a** 800 °C, **b** 900 °C, and **c** 1000 °C.

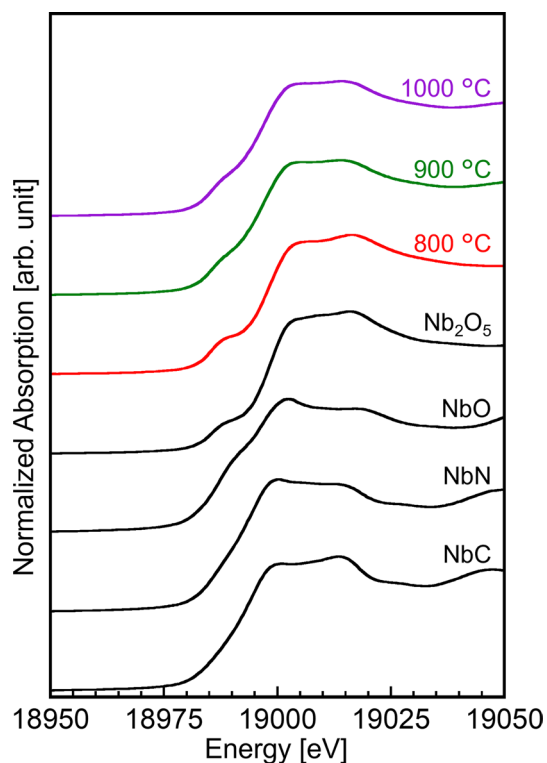


Figure 6 Nb K-edge XANES spectra of the samples obtained by heat-treating the “as irradiated” precursor at different temperatures.

Table 1 Chemical composition of the samples obtained by heat-treating the “as irradiated” precursor calculated from the linear combination fitting analysis

Precursor preparation	Heating temperature	Molecular ratio			
		Nb ₂ O ₅	NbO	NbN	NbC
Irradiation	800 °C	0.90	0.10	0	0
	900 °C	0.59	0	0.41	0
	1000 °C	0.60	0	0.40	0

activity was examined by comparing the ORR activities of these samples.

The SSV graphs of each catalyst are shown in Fig. 7, and Table 2 lists the E_{rest} and i_{ORR} at 0.5 V vs. RHE derived from the SSV data. The E_{rest} and i_{ORR} are similar for both precursor preparation methods. The niobium loading amount, calculated as the metallic niobium equivalent, is thought to differ between the catalysts; however, this difference in content is assumed to have no significant impact on the ORR activity. The crystal phases of the niobium oxynitride nanoparticles are consistent; however, the particle

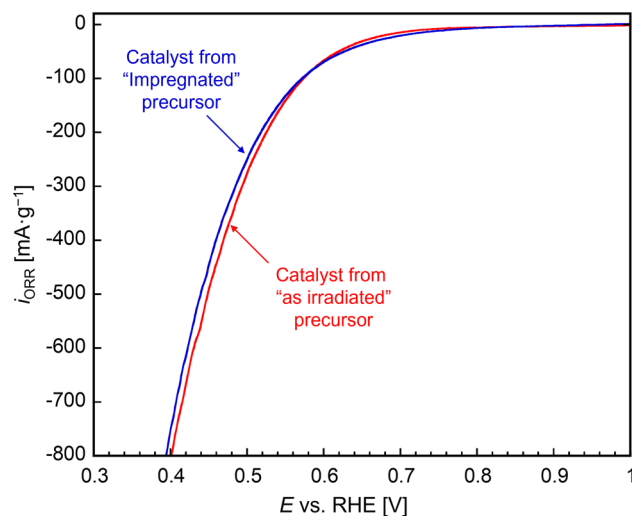


Figure 7 SSV graphs of the samples obtained from the heat treatment of each precursor.

Table 2 E_{rest} and i_{ORR} at 0.5 V vs. RHE derived from the SSV data of the catalyst

Precursor preparation	Heating temperature	i_{ORR} at 0.5 V [mA·g ⁻¹]	E_{rest} (O ₂) [V vs. RHE]
Irradiation	800 °C	−275.3	0.849
	900 °C	−418.6	0.823
	1000 °C	−473.1	0.819
Impregnation	800 °C	−250.0	0.841

sizes differ. Notably, nanosized niobium oxynitrides are known to exhibit ORR activity [12]. In this study, the surface of the niobium oxynitride nanoparticles is also considered the primary active site. These results indicate that an increase in the specific surface area attributed to particle size reduction does not necessarily increase the number of effective active sites. Increasing the specific surface area of catalyst particles can enhance the number of active sites; however, in this study, the reduction in the niobium oxynitride particle size does not improve the ORR activity.

As shown in Fig. 1, the ORR current is generated by electrons moving from the electrode to the active sites on the niobium nanoparticles through macroelectron conduction paths in the carbon support, followed by microelectron conduction paths. Based on this concept, the two catalysts with different particle sizes are compared to discuss the relationship between particle size and conduction paths and evaluate their effect on the ORR activity.

The assumptions considered to define the catalyst model are listed below.

Assumption 1. In both catalysts, niobium-based nanoparticles are dispersed in the same manner on the surface of the carbon support.

Assumption 2. In both catalysts, carbon residues functioning as microelectron conduction paths at the interface between the niobium-based nanoparticles and the carbon support have the same morphological structure.

Assumption 3. The electrical conductivity of niobium-based nanoparticles is low, and only the active sites near the microelectron conduction paths contribute to the ORR activity.

The relationship between the size of the niobium-based nanoparticles and the number of active sites contributing to the ORR was examined based on these assumptions. Detailed calculation procedures are provided in Supporting Information (S3). The results showed that the number of effective active sites did not depend on the size of the niobium-based nanoparticles. Thus, under Assumptions 1–3, reducing the size of niobium-based nanoparticles is not a dominant factor for improving the ORR activity. These findings do not contradict the experimental results obtained in this study.

Refining the parameters defined by the assumptions to address the factor of Assumption 2 is necessary to utilize the increased specific surface area achieved by reducing the size of niobium-based nanoparticles and enhance the ORR activity. If the morphology of the microelectron conduction paths can be precisely controlled, the increase in the specific surface area caused by downsizing can result in a larger interface area between the niobium-based nanoparticles and microelectron conduction paths. Consequently, the number of active sites near the microelectron conduction paths can increase, enhancing the ORR activity. In addition, on optimizing the morphology of the microelectron conduction paths, further improvements in ORR activity can be expected by improving Assumptions 1 and 3.

For Assumption 1, increasing the dispersion of the niobium-based nanoparticles on the conductive support could expose more niobium-based particles on the surface, increasing the number of active

sites. For Assumption 3, controlling the crystal phase and composition of the particles that serve as active sites to improve electrical conductivity could enable sites farther away from the microelectron conduction paths to become functional. If these improvements are achieved, the increased specific surface area caused by downsizing the niobium-based nanoparticles can increase the number of effective active sites.

Effect of catalyst structure on the oxygen reduction reaction activity

The relationships between nitrogen-doping levels, the state of microelectron conduction paths, and their effect on the ORR activity were examined based on the comparison of the samples analyzed in "Effect of heat-treatment temperature on the catalyst structure" section. Figure 8 shows the SSV graphs for each catalyst, and Table 2 lists E_{rest} and i_{ORR} at 0.5 V vs. RHE obtained from the SSV data. Unlike the sample heat-treated at 800 °C, E_{rest} decreased and i_{ORR} increased for the samples heat-treated at 900 and 1000 °C, indicating a trade-off between the E_{rest} and i_{ORR} in the synthesized catalysts. In this study, E_{rest} reflects the quality of the active sites, whereas i_{ORR} indicates both the quality of the active sites and electrical conductivity of the catalyst samples.

According to the chemical composition shown in Table 1, ~ 40% of NbN was confirmed in the samples heat-treated at 900 and 1000 °C, whereas it was absent

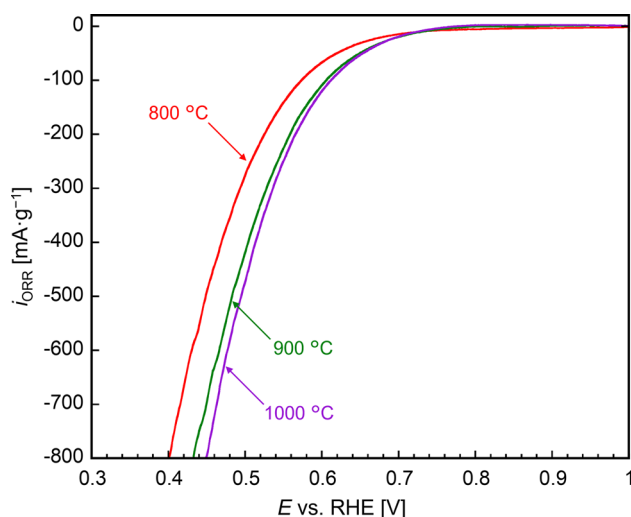


Figure 8 SSV graphs of the samples obtained by heat-treating the “as irradiated” precursor at different temperatures.

in the sample heat-treated at 800 °C. In addition, although the chemical composition obtained from the linear combination fitting of the normalized Nb K-edge XANES standard spectra indicated no nitride in the sample heat-treated at 800 °C, the XRD pattern in Fig. 5 confirmed the presence of a niobium oxynitride crystal phase. These results indicated that nitrogen-doping in niobium oxide particles occurs at all treatment temperatures; however, excessive nitrogen-doping at 900 and 1000 °C, compared to that at 800 °C, resulted in reduced active site quality. This observation aligned with previous studies, thereby indicating the preference for a catalyst with high ORR activity when doping niobium oxide with a small amount of nitrogen [12].

The increase in the i_{ORR} in the samples heat-treated at 900 and 1000 °C compared to the sample heat-treated at 800 °C was attributed to the graphitization of carbon residues formed during PAN addition and heat treatment at high temperatures, which enhanced electrical conductivity. These findings indicated that improving the electrical conductivity of the carbon residues through sufficient graphitization and achieving an optimal amount of nitrogen-doping in the oxide nanoparticles was necessary for achieving high ORR activity in oxide-based catalysts.

Conclusion

Niobium oxynitride nanoparticles with different particle sizes were synthesized on the surface of carbon supports, and the effect of particle size reduction on the ORR activity was examined. The particle size of niobium oxynitride did not necessarily enhance the ORR activity, which was supported by inferences based on the calculation results. However, precisely controlling the morphology of the microelectron conduction paths was deemed necessary to exploit the benefits of particle size reduction and enhance the ORR activity.

This study highlights that, contrary to the conventional expectation of improved catalytic activity through particle size reduction, such an approach is insufficient for oxide-based catalysts with low electrical conductivity. By integrating experimental comparisons of particle size effects with catalyst model calculations, this work underscores the necessity of optimizing microelectron conduction paths to fully

utilize the benefits of particle size reduction, distinguishing it from similar studies.

In addition, the nitrogen-doping on niobium oxide particles became more pronounced with an increase in the heat-treatment temperature. This excessive nitrogen-doping was linked to a decrease in the quality of the active sites, which resulted in a lower rest potential. The enhanced graphitization of carbon residues with an increase in the heat-treatment temperature served as microelectron conduction paths and was presumed to have improved the electrical conductivity. These findings suggest that simultaneously forming highly conductive, graphitized carbon residues and maintaining an optimal level of nitrogen-doping in the oxide nanoparticles is crucial for synthesizing oxide-based catalysts with high ORR activity.

This study provides valuable insights into material design strategies aimed at improving the performance of oxide-based catalysts.

Acknowledgements

The authors thank Koga Isotope Co. Ltd. for their cooperation with the gamma-ray irradiation. XAS experiments were performed at the NW-10A beamline of KEK under the approval of the Photon Factory Program Advisory Committee (Proposal No. 2022G074). This study was supported by JSPS KAKENHI (Grant Nos. 23K04912 and 24KJ1592).

Author contributions

Naoki Shinyoshi, Satoshi Seino, Yuta Hasegawa, and Akimitsu Ishihara were involved in the conceptualization. Naoki Shinyoshi, Yuta Hasegawa, Yuta Uetake, and Takaaki Nagai conducted experiments. Naoki Shinyoshi and Yuta Hasegawa contributed to the data analysis and investigation. Naoki Shinyoshi and Satoshi Seino were involved in the funding acquisition and writing—original draft. Naoki Shinyoshi, Satoshi Seino, Yuta Uetake, Takaaki Nagai, Ryuji Monden, Akimitsu Ishihara, and Takashi Nakagawa contributed to writing—review and editing. Takashi Nakagawa and Satoshi Seino contributed to the resources and supervision.

Funding

Open Access funding provided by Osaka University.

Data availability

Not applicable.

Declarations

Conflicts of interest The authors declare no conflict of interest.

Ethical approval Not applicable.

Supplementary Information The online version contains supplementary material available at <https://doi.org/10.1007/s10853-025-10632-z>.

Open Access This article is licensed under a Creative Commons Attribution 4.0 International License, which permits use, sharing, adaptation, distribution and reproduction in any medium or format, as long as you give appropriate credit to the original author(s) and the source, provide a link to the Creative Commons licence, and indicate if changes were made. The images or other third party material in this article are included in the article's Creative Commons licence, unless indicated otherwise in a credit line to the material. If material is not included in the article's Creative Commons licence and your intended use is not permitted by statutory regulation or exceeds the permitted use, you will need to obtain permission directly from the copyright holder. To view a copy of this licence, visit <http://creativecommons.org/licenses/by/4.0/>.

References

- [1] Rand DAJ, Woods R (1972) A study of the dissolution of platinum, palladium, rhodium and gold electrodes in 1 *m* sulphuric acid by cyclic voltammetry. *J Electroanal Chem and Inter Electrochem* 35:209–218. [https://doi.org/10.1016/S0022-0728\(72\)80308-5](https://doi.org/10.1016/S0022-0728(72)80308-5)
- [2] Whiston MM, Azevedo IL, Litster S, Whitefoot KS, Samaras C, Whitacre JF (2019) Expert assessments of the cost and expected future performance of proton exchange membrane fuel cells for vehicles. *Proc Natl Acad Sci U S A* 116:4899–4904. <https://doi.org/10.1073/pnas.1804221116>
- [3] Madheswaran DK, Jayakumar A (2021) Recent advancements on non-platinum based catalyst electrode material for polymer electrolyte membrane fuel cells: a mini techno-economic review. *Bull Mater Sci* 44:287. <https://doi.org/10.1007/s12034-021-02572-6>
- [4] Nie Y, Li L, Wei Z (2015) Recent advancements in Pt and Pt-free catalysts for oxygen reduction reaction. *Chem Soc Rev* 44:2168–2201. <https://doi.org/10.1039/C4CS00484A>
- [5] Shao M, Chang Q, Dodelet J-P, Chenitz R (2016) Recent advances in electrocatalysts for oxygen reduction reaction. *Chem Rev* 116:3594–3657. <https://doi.org/10.1021/acs.chemrev.5b00462>
- [6] Seo J, Cha D, Takanabe K, Kubota J, Domen K (2013) Electrodeposited ultrafine NbO_x, ZrO_x, and TaO_x nanoparticles on carbon black supports for oxygen reduction electrocatalysts in acidic media. *ACS Catal* 3:2181–2189. <https://doi.org/10.1021/cs400525u>
- [7] Ishihara A, Doi S, Mitsushima S, Ota K (2008) Tantalum (oxy)nitrides prepared using reactive sputtering for new nonplatinum cathodes of polymer electrolyte fuel cell. *Electrochim Acta* 53:5442–5450. <https://doi.org/10.1016/j.electacta.2008.02.092>
- [8] Tominaka S, Ishihara A, Nagai T, Ota K (2017) Noncrystalline titanium oxide catalysts for electrochemical oxygen reduction reactions. *ACS Omega* 2:5209–5214. <https://doi.org/10.1021/acsomega.7b00811>
- [9] Ota K, Ohgi Y, Nam K-D, Matsuzawa K, Mitsushima S, Ishihara A (2011) Development of group 4 and 5 metal oxide-based cathodes for polymer electrolyte fuel cell. *J Power Sources* 196:5256–5263. <https://doi.org/10.1016/j.jpowsour.2010.09.021>
- [10] Ishihara A, Nagai T, Ukita K, Arai M, Matsumoto M, Yu L, Nakamura T, Sekizawa O, Takagi Y, Matsuzawa K, Napporn TW, Mitsushima S, Uruga T, Yokoyama T, Iwasawa Y, Imai H, Ota K (2019) Emergence of oxygen reduction activity in zirconium oxide-based compounds in acidic media: creation of active sites for the oxygen reduction reaction. *J Phys Chem C* 123:18150–18159. <https://doi.org/10.1021/acs.jpcc.9b02393>
- [11] Shinyoshi N, Seino S, Uetake Y, Nagai T, Monden R, Ishihara A, Nakagawa T (2023) Radiation-induced synthesis of carbon-supported niobium oxide nanoparticle catalysts and investigation of heat treatment conditions to improve the oxygen reduction reaction activity. *J Ceram Soc Jpn* 131:575–580. <https://doi.org/10.2109/jcersj2.23039>

- [12] Seo J, Moon W-J, Jung W-G, Park J-W (2022) A N-doped NbO_x nanoparticle electrocatalyst deposited on carbon black for oxygen reduction and evolution reactions in alkaline media. *Mater Adv* 3:5315–5324. <https://doi.org/10.1039/D2MA00292B>
- [13] Bolokang AS, Phasha MJ (2010) Formation of titanium nitride produced from nanocrystalline titanium powder under nitrogen atmosphere. *Int J Refract Met Hard Mater* 28:610–615. <https://doi.org/10.1016/j.ijrmhm.2010.05.008>
- [14] Zukalova M, Prochazka J, Bastl Z, Duchoslav J, Rubacek L, Havlicek D, Kavan L (2010) Facile conversion of electrospun TiO₂ into titanium nitride/oxytitanium nitride fibers. *Chem Mater* 22:4045–4055. <https://doi.org/10.1021/cm100877h>
- [15] Ishihara A, Arao M, Matsumoto M, Tokai T, Nagai T, Kuroda Y, Matsuzawa K, Imai H, Mitsushima S, Ota K (2020) Niobium-added titanium oxides powders as non-noble metal cathodes for polymer electrolyte fuel cells—electrochemical evaluation and effect of added amount of niobium. *Int J Hydrog Energy* 45:5438–5448. <https://doi.org/10.1016/j.ijhydene.2019.08.217>
- [16] Uehara N, Ishihara A, Imai H, Matsumoto M, Arao M, Ohgi Y, Kohno Y, Matsuzawa K, Mitsushima S, Ota K (2015) Oxide-based electrocatalysts toward oxygen reduction reaction as non Pt cathodes for PEFC. *ECS Trans* 64:23–31. <https://doi.org/10.1149/06436.0023ecst>
- [17] Denton AR, Ashcroft NW (1991) Vegard's law. *Phys Rev A* 43:3161–3164. <https://doi.org/10.1103/PhysRevA.43.3161>

Publisher's Note Springer Nature remains neutral with regard to jurisdictional claims in published maps and institutional affiliations.